Initial stages of Mn adsorption on Ge(111)

Changgan Zeng,[1] Wenguang Zhu,[2,3] Steven C. Erwin,[4] Zhenyu Zhang,[1,2,5] and Hanno H. Weitering[1,2]
[1]*Department of Physics and Astronomy, The University of Tennessee, Knoxville, Tennessee 37996, USA*
[2]*Condensed Matter Sciences Division, Oak Ridge National Laboratory, Oak Ridge, Tennessee 37831, USA*
[3]*International Center for Quantum Structures and Institute of Physics, Chinese Academy of Sciences, Beijing 100080, People's Republic of China*
[4]*Center for Computational Materials Science, Naval Research Laboratory, Washington, DC 20375, USA*
[5]*Department of Physics and Division of Engineering and Applied Sciences, Harvard University, Cambridge, Massachusetts 02138, USA*
(Received 23 February 2004; revised manuscript received 2 June 2004; published 29 November 2004)

The initial stages of growth of Mn on Ge(111) were studied with scanning tunneling microscopy, x-ray photoelectron spectroscopy, and first-principles density functional theory calculations. Mn atoms adsorb on the H_3 sites of the Ge(111)-$c(2\times8)$ reconstruction, a process that is usually accompanied by a registry shift (along the $[\bar{1}10]$ direction) of an adjacent Ge adatom row. Deposition of approximately one monolayer of Mn and subsequent annealing results in the formation of Mn_5Ge_3 islands. Epitaxial Mn_5Ge_3 *films* can be grown from a solid-state reaction between the Mn deposit and Ge substrate. The Mn_5Ge_3 films are ferromagnetic metals with a magnetic moment of 2.6 μ_B per Mn, as determined from the Mn 3*s* exchange splitting in XPS. Theoretical calculations of the adsorption sites, surface structures, and electronic structure all agree exceedingly well with the experimental observations.

DOI: 10.1103/PhysRevB.70.205340 PACS number(s): 68.43.Fg, 68.43.Bc, 68.37.Ef, 75.50.Pp

I. INTRODUCTION

Semiconductor spintronics is a burgeoning field in solid-state research. It has presented the research community with numerous scientific challenges ranging from questions of how to understand and control spin-dependent transport through interfaces to the more basic materials issues, specifically those that relate growth and processing with magnetism and transport. The promise is a whole new generation of spin-based electronic devices with enhanced functionality, higher speeds, and reduced power consumption.[1] Dilute magnetic semiconductors (DMS) are particularly interesting materials. They can easily be integrated into semiconductor heterostructures and spin injection from a DMS source electrode may be very efficient because of the natural impedance match to the semiconductor channel.

In recent years, most research on DMS materials focused on Mn doped III-V semiconductors.[2–4] Recently, researchers have succeeded in kinetically stabilizing ferromagnetic Ge on Ge(001) and GaAs(001) by molecular beam epitaxial (MBE) growth of Ge, while coevaporating a few percent of Mn.[5] The ferromagnetic Curie temperature (T_c) of the Mn_xGe_{1-x} films can reach 116 K ($x=0.05$).[5] The advantage of germanium is that it is fully silicon compatible, unlike III-V semiconductors. Furthermore, doping control in Si and Ge should be less complicated than in III-V semiconductors. It should therefore be easier to control the chemistry, the Mn-lattice locations, and growth of Mn:Ge, which in turn should lead to a better understanding of the origins of collective ferromagnetism in DMS compounds.

To analyze Mn diffusion and incorporation during Mn_xGe_{1-x} growth, it is very important to investigate the structure and growth of Mn on various Ge substrates in a typical surface science setup. In this paper we present a comprehensive study of the growth of Mn on Ge(111), using scanning tunneling microscopy (STM), x-ray photoelectron spectroscopy (XPS), and density functional theory (DFT). The Mn site locations, spatial distribution, and the electronic properties are investigated in great detail. Temperature is a very critical parameter that controls intermixing of Mn and Ge. At typical MBE growth temperatures, uniform Mn_5Ge_3 clusters easily form for a wide range of Mn coverage. These clusters are in fact epitaxial which can be understood from the close lattice match between the $Mn_5Ge_3(0001)$ hexagonal basal plane and the Ge(111) substrate.[6] In this way, we have successfully grown epitaxial Mn_5Ge_3 films on Ge(111) by annealing as-deposited Mn films between 300 and 650 °C. We furthermore investigated the electronic and magnetic properties during the initial stages of interface formation. The experimental results are well explained from DFT calculations.

II. EXPERIMENTAL AND COMPUTATIONAL PROCEDURES

Mn was deposited in a MBE system with a base pressure of 4.0×10^{-11} mbar. Ge(111) substrates were cleaned *in situ* by several circles of Ne-ion sputtering and annealing to 650 °C. Mn atoms were evaporated from a pyrolytic boron nitride crucible. Epitaxial Mn_5Ge_3 films were produced by room temperature deposition of a few layers of Mn, followed by a several-minute anneal at 650 °C, a process known as solid phase epitaxy. Annealing temperatures between 300 and 650 °C always produces uniform Mn_5Ge_3 films. The surfaces were characterized *in situ* by variable-temperature STM, reflection high energy electron diffraction (RHEED), and XPS with monochromatic Al $K\alpha$ radiation (1486.6 eV).

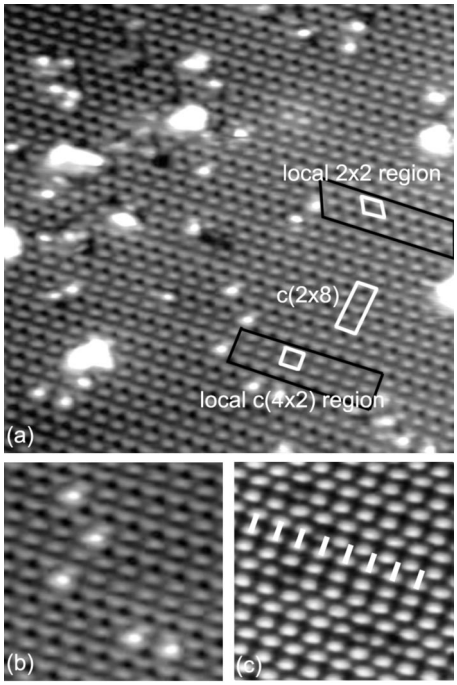

FIG. 1. (a) Typical STM image (20 nm×20 nm) of 0.04 ML Mn on Ge(111) recorded at a sample bias of −1.6 V. (b) and (c) are the magnified images (7 nm×7 nm), recorded in the dual bias mode with sample biases of −1.6 and +1.6 V, respectively. The white guidelines in (c) facilitate the observation of the adatom row shift.

Spin-polarized DFT calculations[7–9] within the generalized-gradient approximation[10] were performed to calculate the adsorption energies of Mn on Ge(111)-$c(2\times8)$ and to simulate the STM images of the Mn_5Ge_3 alloy films. The adsorption energies were calculated using a large supercell, corresponding to two $c(2\times8)$ unit cells, and consisting of six layers with sixteen Ge atoms each. Four Ge atoms are placed at the T_4 sites of the top surface and 16 hydrogen atoms passivate the bottom of the slab. Consecutive slabs are separated by 13 Å of vacuum. Atoms of the bottom two Ge layers are fixed at the corresponding bulk positions, while the other atoms are fully relaxed. Full relaxation was performed using ultrasoft pseudopotentials (energy cutoff 227 eV) and 3×3 *k*-point sampling. For the STM simulations of Mn_5Ge_3, seven-layer symmetric slabs separated by 10 Å of vacuum were used; full relaxation was performed using projector-augmented-wave potentials (with energy cutoff 280 eV) and 4×4 *k*-point sampling. Constant-current STM images were simulated using the approach of Tersoff and Hamann.[11]

III. RESULTS AND DISCUSSION

A. Manganese chemisorption

Figure 1(a) shows a STM image of 0.04 ML of Mn on Ge(111), deposited at room temperature (RT). About 70% of the Mn atoms are distributed randomly on the surface, while the remaining Mn atoms aggregate into small clusters of monolayer height. Dual-bias STM images are shown in Figs. 1(b) and 1(c). The Ge(111)-$c(2\times8)$ structure is atomically resolved which is composed of two alternating rows of 2×2 and $c(4\times2)$ subunit cells, and accompanied by local 2×2 and $c(4\times2)$ regions.[12–14] Rest atoms are the dominant features in the filled-state (negative-bias) image, while adatoms dominate at positive bias.[12,13] Isolated Mn atoms show up as bright protrusions in filled-state images and dark depressions in empty-state images.

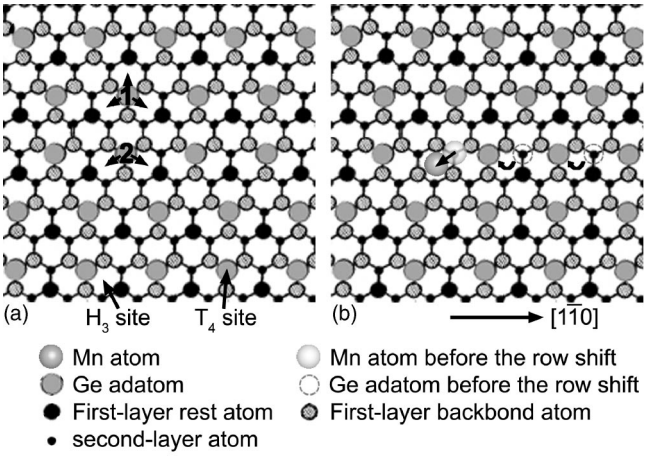

FIG. 2. (a) Top view of the Ge(111)-$c(2\times8)$ surface structure. Two inequivalent adatom sites are labeled 1 and 2. The Mn atom on site 1 can hop to three adjoining H_3 sites; the Mn atom on site 2 can only hop to two neighboring H_3 sites because there are only two neighboring rest atoms instead of three. (b) Model for the Mn adsorption mechanism: A Mn atom replaces a T_4 Ge adatom, and then shifts to the adjacent H_3 site. This leaves an open T_4 adatom site, which triggers the registry shift of the adjacent row of Ge adatoms.

An individual Mn atom is located in between two Ge rest atoms though slightly displaced in the direction perpendicular to the rest atom row [see "restatom image" Fig. 1(b)]. It is also located in between two Ge adatoms in the adatom row, also with a slight perpendicular displacement [see "adatom image" Fig. 1(c)]. Considering the well-established structure of the Ge(111)-$c(2\times8)$ reconstruction [Fig. 2(a)],[12–14] it is concluded that the threefold H_3 site must be the only Mn adsorption site in all of our STM images. Surprisingly, in most cases Mn adsorption is accompanied by a registry shift of an adjacent row of Ge adatoms along the $[1\bar{1}0]$ direction as indicated by the short white markers in Fig. 1(c). The shift of the adatom row is naturally accompanied by a registry shift of the rest-atom row [see Figs. 1(b) and 1(c)]. It is not possible to determine which direction the adatom row has shifted because the coexisting 2×2 and $c(4\times2)$ adatoms arrangements on Ge(111) add additional complexity that precludes such analysis.[12] Deposition experiments at low temperature (167 and 76 K) produced identical results.

If we assume that the Mn atoms adsorb directly at the H_3 sites, it is hard to understand why an entire adatom row would be shifted. We propose a plausible mechanism which is similar to the atomic motion of Pb on Ge(111).[14] First, a Mn atom replaces a Ge adatom at the T_4 site, and then shifts to a neighboring H_3 site (Fig. 2; the ejected Ge atom may diffuse to a step edge). The possible directions of the shift

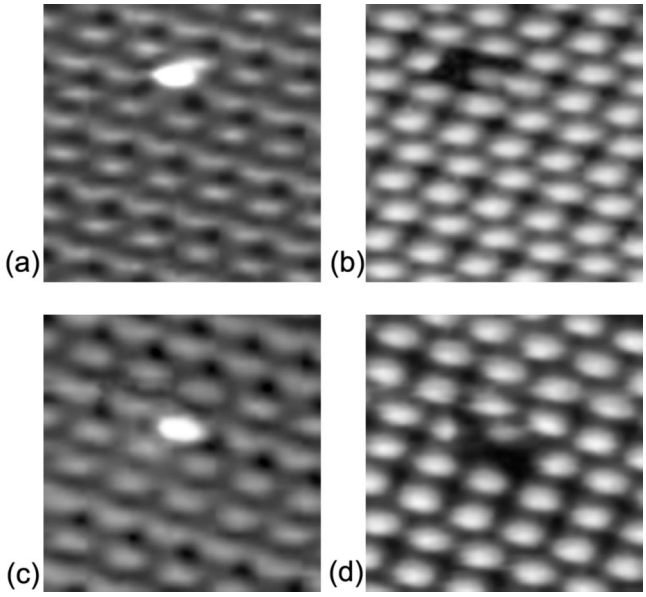

FIG. 3. STM images showing Mn adsorption without Ge adatom row shift. (a) and (b) are dual bias STM images (4 nm $\times$4 nm) recorded at a sample bias of −1.6 and 1.6 V, respectively. (c) and (d) present another pair of dual bias STM images (4 nm $\times$4 nm) recorded at a sample bias of −1.6 and +1.6 V, respectively. Mn adatoms appear bright in filled state images and dark in empty state images.

are indicated in Fig. 2(a) (Mn atoms rarely shift in the direction perpendicular to the Ge adatom row, which runs along the $[1\bar{1}0]$ direction).[14] The Mn displacement toward the H_3 site creates a vacancy at the original T_4 site, which in turn allows the hopping of Ge adatoms along the $[1\bar{1}0]$ direction. The adatom row shift usually terminates at a defect site or another Mn site.

We note that the imaging contrast of the Ge adatoms and rest atoms next to a Mn site has not changed appreciably (Fig. 1), suggesting that there is no obvious charge transfer between the Mn atoms and neighboring Ge dangling bonds. Furthermore, it can be stated that Mn adsorption does not significantly affect the charge transfer between the Ge adatoms and rest atoms. These observations are clearly different from the cases of H and Ga adsorption on Ge(111) where contrast variations are evident.[15,16] In rather exceptional cases, we can identify H_3 Mn chemisorption sites without the usual registry shift of adjacent adatom rows (Fig. 3). The example in Figs. 3(c) and 3(d) is exceptional though and these adsorption states should thus be metastable. We also note that these states are absent for Pb on Ge(111).[14]

TABLE I. Adsorption energies of a Mn adatom on Ge(111)-$c(2\times8)$, in electron volts. The adsorption energy is referenced with respect to the energies of a free Mn atom and clean Ge(111)-$c(2\times8)$ structure.

Adsorption site	Adsorption energy	Adsorption site	Adsorption energy
H_3^1	−2.38	T_4^1	−1.94
H_3^2	−2.38	T_4^2	−1.94
H_3^3	−2.38	T_4^3	−1.93
H_3^4	−2.38	T_4^4	−1.91
H_3^5	−2.38	T_4^5	−1.87
H_3^6	−2.22	T_4^6	−1.87
H_3^7	−2.18		
H_3^8	−2.18		

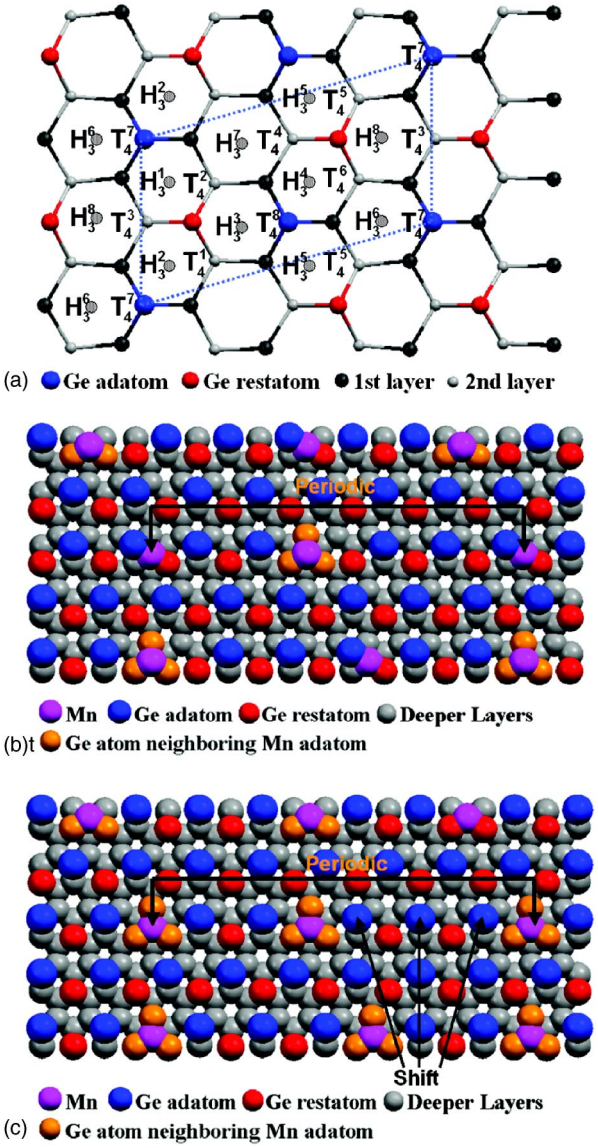

FIG. 4. (Color online) Top view of the Ge(111)-$c(2\times8)$ surface (a). The various adsorption sites are labeled and their total energies are indicated in Table I. Atomic structure before (b) and after (c) the Ge adatom row shift, using a 6×8 super cell.

The relative adsorption energy of Mn was calculated for the various adsorption sites within the $c(2\times8)$ unit cell. The results are listed in Table I.[17] The most likely chemisorption sites on the diamond-type (111) surfaces are the threefold coordinated T_4 and H_3 sites that are located above the second and fourth Ge layer, respectively. The Ge adatoms of the $c(2\times8)$ structure are placed on the T_4^7 or T_4^8 sites [Fig. 4(a)]. Among the eight H_3 sites per primitive $c(2\times8)$ unit

TABLE II. Comparison of DFT results for substitutional and nonsubstitutional Mn adsorption on Ge(111)-$c(2\times8)$. Energies are given in electron volts.

	Type A: Ge adatom at T_4^7 site		Type B: Ge adatom at T_4^8 site	
	Mn adsorption site	Adsorption energy	Mn adsorption site	Adsorption energy
Case 1	H_3^1, H_3^2	−2.38	H_3^4, H_3^5	−2.38
	H_3^6	−2.22	H_3^3	−2.38
Case 2	Substitutional Mn at T_4 adatom site			
	T_4^7	−2.36	T_4^8	−2.38
Case 3	Substitutional Mn shifted from T_4 adatom site to neighboring H_3 site			
	Original adatom site: T_4^7		Original adatom site: T_4^8	
	H_3^1, H_3^2	−2.58	H_3^4, H_3^5	−2.58
	H_3^6	−2.45	H_3^3	−2.56

cell, five of these turn out to have nearly identical adsorption energies. These sites are labeled H_3^1, H_3^2, H_3^3, H_3^4, and H_3^5. These sites all have one neighboring Ge adatom and one neighboring rest atom. Mn adsorption on the remaining three H_3 sites (H_3^6, H_3^7, and H_3^8) is less favored by approximately 0.16–0.20 eV. The difference between the most stable H_3 sites and the T_4 sites is about 0.45 eV. These results are fully consistent with the experimental results. For instance, by comparing the filled-state rest atom and empty-state adatom images in Figs. 1 and 3 one observes that the Mn atoms are located in between a Ge adatom and a rest atom. Notice that only the H_3^1 through H_3^5 sites are located in between two dangling bond orbitals (from the Ge adatom and rest atom). H_3^6 only has one neighboring adatom but no rest atom whereas H_3^8 only has one neighboring rest atom but no adatom. H_3^7 has no dangling-bond neighbors at all. Evidently, Mn prefers to be coordinated with two dangling bonds, rather than one or zero dangling bonds, presumably because it would allow hybridization with the adatom–rest atom "bond."

We also investigated the possibility of substitutional adsorption and compared the following configurations: (1) a Mn adatom at the most stable adsorption site neighboring the T_4^7 or T_4^8 Ge adatom; (2) a Mn adatom substituting a Ge adatom (i.e., Ge atom removed); and (3) a Mn adatom substituting a T_4^7 or T_4^8 Ge adatom, followed by a hop to a neighboring H_3 site. [Strictly speaking, the third scenario is just an *interpretation* of the STM images (Fig. 2); the DFT calculation of course does not address such dynamics.] In order to compare the relative stabilities of these three different cases, we must account for the chemical potential of Ge because the number of Ge atoms is different in each case. We referenced the chemical potential of Ge to the total energy per Ge atom of bulk Ge. The DFT results are consistent with the proposed scenario of a Mn adatom substituting a Ge adatom, followed by a hop to a neighboring H_3 site. Details are summarized in Table II. Of all six H_3 sites neighboring a Ge adatom site, only the H_3^6 site is not a preferred Mn adsorption site. The favored H_3 sites all have a neighboring rest atom. These results are fully consistent with the case of Pb/Ge(111)-$c(2\times8)$.[14]

In order to understand the observed adatom row shifts, we use a large (6×8) super cell containing 350 atoms. Considering the DFT and experimental results discussed earlier and the computational requirement to maintain a periodic structure, we included two Mn atoms per super cell. One Mn adatom is placed at the most stable adsorpsion site (see Table II); the other Mn adatom substitutes a "same row" Ge adatom and is also subsequently shifted a neighboring H_3 site. We compare the total energy of the configuration with and without the adatom shifts; the detailed atomic structures are shown in Figs. 4(b) and 4(c). The calculation results confirm that the adatom row shift lowers the total energy by about 0.2 eV (due to computational limitations, we only included three shifted adatoms; longer rows would require even larger supercells). Evidently, the adatom row shift can be captured with the DFT using a relatively small super cell. This suggests that the driving force for the motion of adatoms over large distances is not necessarily long range.

Scanning tunneling spectroscopy (STS) data were obtained from single chemisorbed Mn atoms and from pristine Ge(111)-$c(2\times8)$. The averaged point spectra are shown in Fig. 5 and the corresponding dI/dV-V curves are displayed in the inset. Assuming that the density of states (DOS) of the tip is relatively flat near the Fermi level (E_F), dI/dV will be proportional to the local density of states.[11,18] The pristine surface reveals a tunneling gap of about 0.6 eV, which agrees with previous STS results[12] and with the magnitude of the bulk band gap. The current–voltage (I-V) curve from

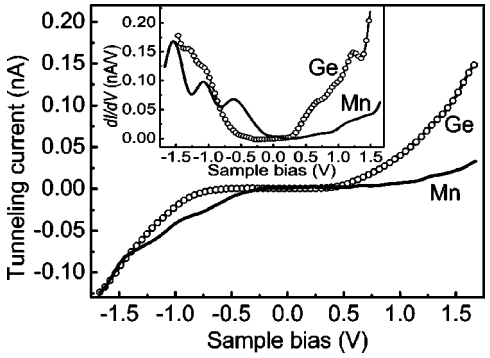

FIG. 5. Averaged I-V curves measured on clean Ge(111)-$c(2\times8)$ and on isolated Mn adatoms. The inset shows the first derivatives of the I-V curves.

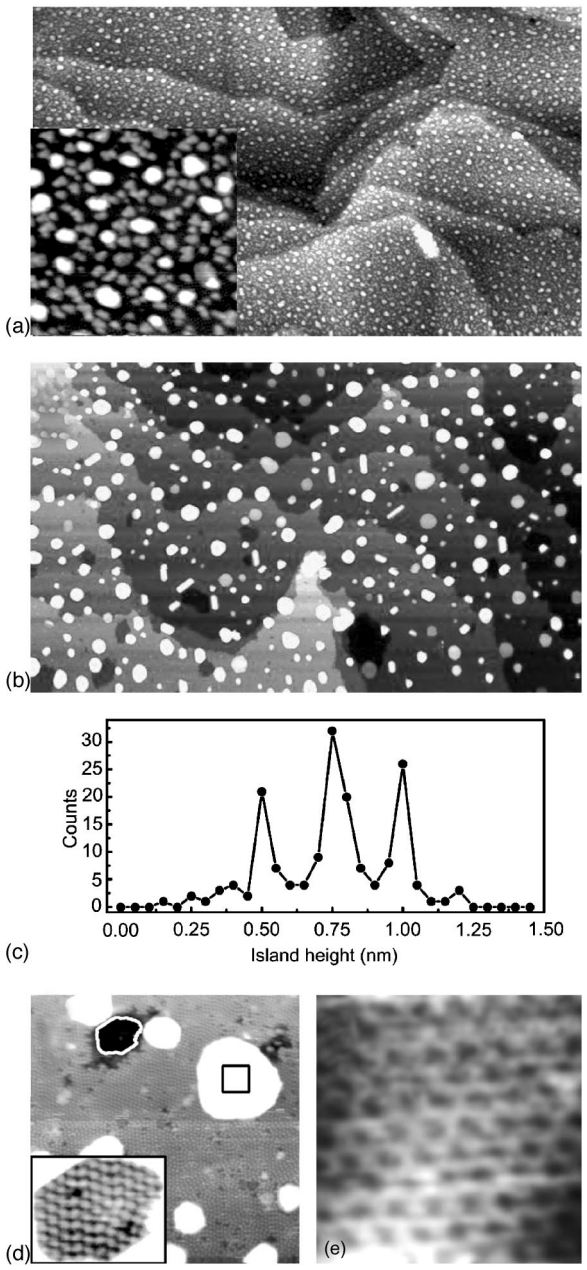

FIG. 6. (a) Large scale STM images (500 nm × 300 nm) of as-deposited Mn on Ge(111)-$c(2\times8)$. The coverage is approximately 1 ML. The inset is a close-up view of 40 nm × 40 nm; (b) 500 nm × 300 nm STM image after annealing to 400 °C. (c) Statistical distribution of the island heights in (b); and (d) close-up view (50 nm × 50 nm) of the annealed sample in (b). The inset shows the enlarged image of the depressed region in the upper left hand corner with adjusted gray scale. (e) Atomically resolved STM image from the area within the rectangular box in (d). The sample bias is +1.8 V for all images.

isolated Mn adatoms shows significant asymmetry around zero bias. The asymmetry in the tunneling current is consistent with the appearance of the Mn atoms in topographic imaging, namely protruding at negative sample bias and depressed at positive sample bias. The occupied states in the dI/dV spectrum reveal distinct peaks at −1.4, −1.0, and −0.6 eV, respectively. These equidistant peaks do not correspond to the known acceptor levels of Mn dopants in bulk Ge which are located at 0.16 eV above the valence band maximum and 0.37 eV below the conduction band minimum.[19] The regular peak spacing cannot correspond to atomic energy levels and is reminiscent of a Coulomb blockade phenomenon. The fact that these peaks are easily observed at room temperature is indicative of Hubbard type repulsions between localized charges within a nanoscale radius from the tunnel junction.[20]

B. Adsorbate clusters and thin films

We now turn to higher coverage. Figure 6(a) shows a large-scale image of as deposited Mn on Ge(111) near RT. The coverage is approximately 1 ML. One clearly observes three-dimensional Mn clusters with a size distribution that is roughly bimodal (about 1.2 and 3.2 nm in diameter; see inset). Large clusters are accompanied by neighboring voids on the Ge(111) surface which may indicate that the larger clusters are manganese germanides (though the composition ratio cannot be determined), while the smaller ones are probably pure Mn.

After annealing at about 400 °C, islands of irregular shape coexist with well defined nanocrystals; the pristine areas still correspond to Ge(111)-$c(2\times8)$ [see Figs. 6(b) and 6(d)]. It is noted that depressed regions or "craters" are also present on the surface. The crater depth is 0.33 nm which is close to the Ge(111) interlayer spacing. Inside these craters, local structures such as 2×2, $c(4\times2)$, or $c(2\times8)$ can still be resolved by STM [see the inset of Fig. 6(d)]. The presence of voids in the substrate surface clearly indicates that Ge atoms are incorporated into the islands, in addition to the Mn atoms. Similar behavior has been observed during Mn deposition onto Si(111).[21,22] Statistical data of the island height distribution are shown in Fig. 6(c). There are three peaks, located at 0.50, 0.75, and 1.0 nm, with a uniform spacing of 0.25 nm. This spacing is not consistent with the Ge(111) layer spacing of 0.327 nm or any known lattice spacing in α-Mn.

Figure 6(e) is a close-up STM image of the area that is indicated by a square box in Fig. 6(d). This area rises 1.0 nm above the $c(2\times8)$ substrate. Atomically resolved images clearly reveal a $(\sqrt{3}\times\sqrt{3})R30°$ honeycomb structure. This image is identical to that of a $Mn_5Ge_3(0001)$ thin film alloy.[6] Evidently, these islands are composed of Mn_5Ge_3. This also explains the 0.25 nm spacing between the various island heights in Fig. 6(c). The unit cell of the Mn_5Ge_3 structure contains four atomic layers that are stacked along the [0001] direction. The $z=0$ and $z=1/2$ planes contain only Mn atoms whereas the $z=1/4$ and $z=3/4$ contain Mn and Ge atoms in equal amounts. Accordingly, there are two possible surface terminations (Mn termination or mixed Mn/Ge termination). The observed island height is exactly half the lattice constant along [0001].[6]

Deposition of a thick Mn film on Ge(111) surface, followed by annealing to 400 °C, always results in the formation of a well-defined Mn_5Ge_3 thin film.[6] Large-scale images of approximately 25 nm thick Mn_5Ge_3 films are shown in Fig. 7(a). Large terraces with occasional screw dislocations

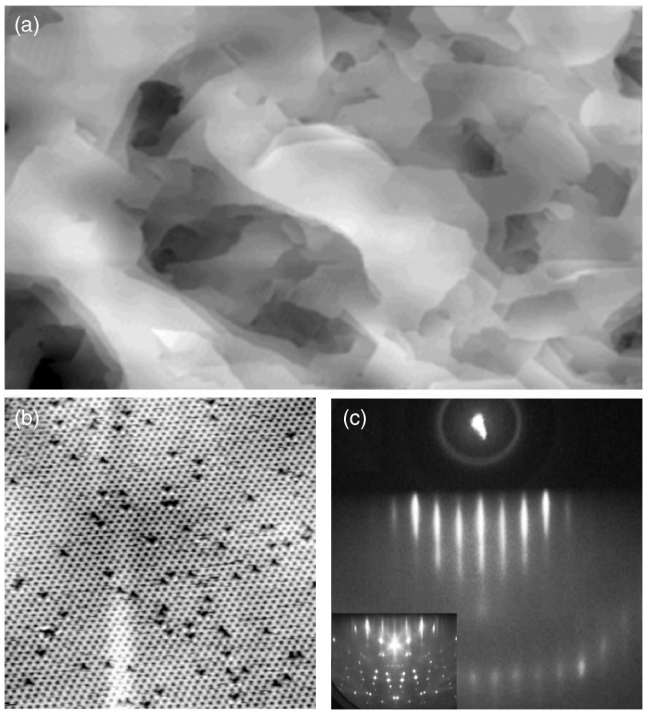

FIG. 7. (a) Large scale STM images (500 nm × 300 nm), recorded with a sample bias of 1.8 V, from the surface of a 25 nm thick Mn_5Ge_3 film. (b) 28 nm × 28 nm STM image with a sample bias of 1.5 V. (c) $(\sqrt{3}\times\sqrt{3})R30°$ 15 keV RHEED pattern of a 25 nm thick Mn_5Ge_3 film with the incident beam along the $[11\bar{2}]$ direction. The inset shows the RHEED pattern of clean Ge(111) $c(2\times8)$.

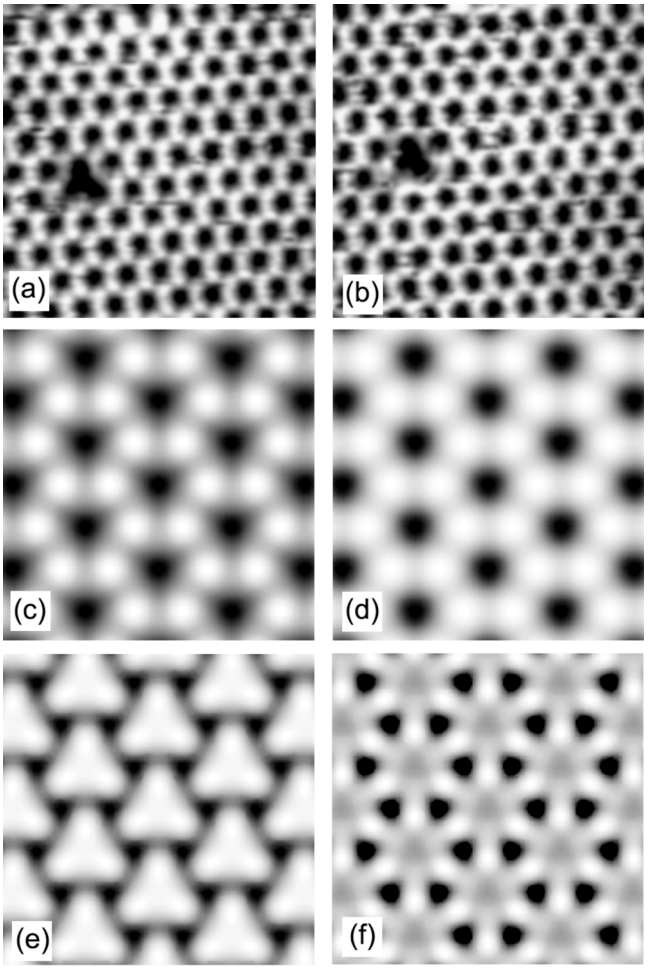

FIG. 8. (a) and (b) are 6.7 nm × 6.7 nm dual bias STM images from a Mn_5Ge_3 film, recorded at a sample bias of −1.5 and +1.5 V, respectively. (c) and (d) are the DFT simulated filled and empty STM images for the Mn-terminated surface. (e) and (f) are the DFT simulated filled and empty STM images for the mixed Mn/Ge termination.

are observed. The latter originate from the 3.7% mismatch between the Ge(111) and $Mn_5Ge_3(0001)$ lattices. Figure 7(b) displays a small scale STM image with the $(\sqrt{3}\times\sqrt{3})R30°$ honeycomb structure with a 4% point-defect density. RHEED patterns along $[11\bar{2}]$ direction, shown in Fig. 7(c), display sharp $(\sqrt{3}\times\sqrt{3})R30°$ streaks, consistent with the STM measurements.

Figures 8(a) and 8(b) show the typical dual-bias STM images of $Mn_5Ge_3(0001)$. Both polarities reveal identical $(\sqrt{3}\times\sqrt{3})R30°$ honeycomb structures. As mentioned before, there are two possible surface terminations along the $Mn_5Ge_3[0001]$ direction: a Mn-terminated surface or a mixed Mn/Ge termination.[6] In order to determine the observed surface termination, DFT calculations for both possible terminations were performed. STM images were simulated using the method of Tersoff and Hamann.[11] The calculated image of the mixed Mn/Ge termination yields a rather complicated hexagonal pattern for both tunneling polarities, with the bright spots located on the Ge atoms. The simulated image for the Mn-terminated reveals a honeycomb pattern for both tunneling polarities, with the bright spots located on the Mn surface atoms. The latter is in excellent agreement with the experimental images. So the surface of Mn_5Ge_3 films is terminated by Mn.

The *I-V* curve from the Mn_5Ge_3 surface has a nonzero slope around zero bias, which is characteristic of a metal [Fig. 9(a)]. XPS spectra from the valence band region show a clear Fermi edge thus confirming metallic behavior; the Fermi edge of a thick Mn film is shown for comparison [Fig. 9(b)]. The two peaks at 1.6 and 4.7 eV binding energy as well as the depressed region from 7.4 to 6.3 eV are perfectly reproduced by the total DOS from the LSDA calculations (Fig. 9).

Figure 10 shows the XPS Mn 3*s* spectrum from Mn_5Ge_3 thin films. A satellite peak is observed at higher binding energy, which arises from the exchange interaction between the unpaired 3*d* electrons and the 3*s* photo hole.[23,24] In the *simplest scenario* of unscreened intra-atomic multiplet splitting, the intensity ratio of the ^5S and ^7S final states should be equal to the ratios of their spin multiplicity, namely $S/(S+1)$ or $\mu/(\mu+2)$, where μ is the magnetic moment per Mn atom.[25] We fitted the two peaks with a Doniach-Šunjić line shape, after subtracting a Shirley background.[26,27] From the fitted intensity ratio, we obtain $\mu=2.6\ \mu_B$ which, considering the simplicity of the atomic multiplet description, is unexpectedly close to the LSDA result and the superconducting quantum interference device (SQUID) measurement in Ref. 6.

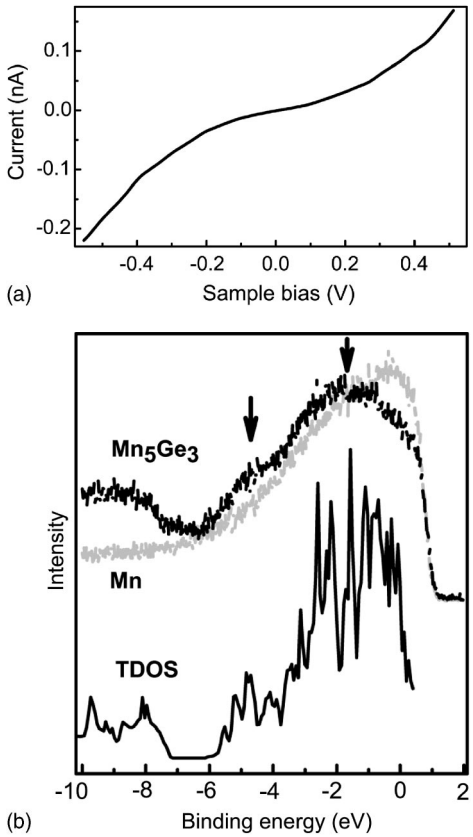

FIG. 9. (a) STS from the surface of $Mn_5Ge_3(0001)$. (b) Valence band XPS spectra near the Fermi energy from as-deposited Mn and from Mn_5Ge_3. The LSDA *total* DOS of bulk Mn_5Ge_3 is shown at the bottom.

The magnitude of the exchange splitting should in principle be proportional to $(2S+1)$ but for 3*d* transition metal compounds, the calculated splittings are usually too large.[23,24] There exists, however, an empirical, linear relationship between the 3*s* exchange splitting and formal valence of Mn ions in a wide variety of *ionic* Mn compounds.[28] From the observed exchange splitting of 4.2 eV and this empirical relation, we also obtained a moment of 2.6 μ_B per Mn atom.

IV. SUMMARY AND CONCLUSIONS

In summary, during submonolayer growth of Mn on Ge(111), Mn atoms preferentially adsorb on the H_3 sites; the adsorption is usually accompanied by a Ge adatom row shift. Annealing of the Mn deposit leads to the formation of epitaxial Mn_5Ge_3. There are no ordered Mn/Ge(111) submonolayer phases. Thick Mn_5Ge_3 films can be grown epitaxially by annealing as-deposited Mn, a process known as solid phase epitaxy. The Mn_5Ge_3 films are terminated with a honeycomb layer of Mn atoms. The films are metallic and according to XPS the magnetic moment per Mn is 2.6 μ_B, in good agreement with the LSDA calculations and with SQUID measurements on thick films. Overall, there is excellent agreement between experimental observations and theoretical calculations.

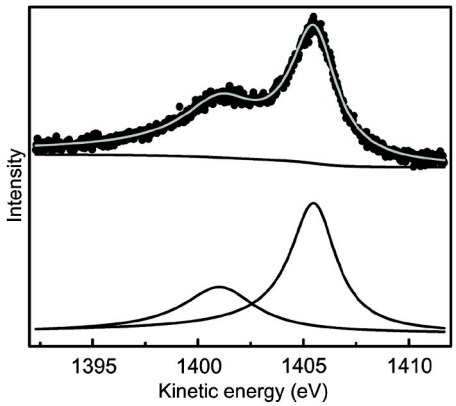

FIG. 10. Mn 3*s* core-level spectrum recorded from Mn_5Ge_3 thin films. The solid line through the data points represents the Doniach-Šunjić fit. The individual ^7S and ^5S components and Shirley background are also shown. The Doniach-Šunjić dimensionless asymmetry parameter is 0.06 for both peaks. The Lorentzian full width at half maximum (FWHM) is 2.4 and 4.0 eV for the ^7S and ^5S components, respectively. The Gaussian FWHM is 0.4 eV.

ACKNOWLEDGMENTS

The authors enjoyed many helpful discussions with Professor E. Kaxiras. This work was sponsored primarily by NSF under Contract No. DMR-0306239 (FRG), and in part by the Department of Energy under Contract No. DE-FG03-02ER45958. Oak Ridge National Laboratory is managed by UT-Battelle, LLC, for the US Department of Energy under Contract No. DE-AC-05-00OR22725.

[1] S.A. Wolf, D.D. Awschalom, R.A. Buhrman, J.M. Daughton, S. von Molnár, M.L. Roukes, A.Y. Chtchelkanova, and D.M. Treger, Science **294**, 1488 (2001).
[2] H. Munekata, H. Ohno, S. von Molnár, A. Segmüller, L.L. Chang, and L. Esaki, Phys. Rev. Lett. **63**, 1849 (1989).
[3] H. Ohno, A. Shen, F. Matsukura, A. Oiwa, A. Endo, S. Katsumoto, and Y. Iye, Appl. Phys. Lett. **69**, 363 (1996).
[4] H. Ohno, Science **281**, 951 (1998).
[5] Y.D. Park, A.T. Hanbicki, S.C. Erwin, C.S. Hellberg, J.M. Sullivan, J.E. Mattson, T.F. Ambrose, A. Wilson, G. Spanos, and B.T. Jonker, Science **295**, 651 (2002).
[6] C. Zeng, S.C. Erwin, L.C. Feldman, A.P. Li, R. Jin, Y. Song, J.R. Thompson, and H.H. Weitering, Appl. Phys. Lett. **83**, 5002 (2003).
[7] G. Kresse and J. Hafner, Phys. Rev. B **47**, 558 (1993); **49**, 14 251 (1994).
[8] G. Kresse and J. Furthmüller, Comput. Mater. Sci. **6**, 15 (1996).
[9] G. Kresse and J. Furthmüller, Phys. Rev. B **54**, 11 169 (1996).
[10] J.P. Perdew, in *Electronic Structure of Solids '91*, edited by P. Ziesche and H. Eschrig (Akademie Berlin, 1991); J.P. Perdew

and Y. Wang (unpublished).
[11] J. Tersoff and D.R. Hamann, Phys. Rev. Lett. **50**, 1998 (1983).
[12] R.S. Becker, B.S. Swartzentruber, J.S. Vickers, and T. Klitsner, Phys. Rev. B **39**, 1633 (1989).
[13] E.S. Hirschorn, D.S. Lin, F.M. Leibsle, A. Samsavar, and T.-C. Chiang, Phys. Rev. B **44**, 1403 (1991).
[14] I.-S. Hwang and J. Golovchenko, Science **258**, 1119 (1992).
[15] G. Lee, H. Mai, I. Chizhov, and R.F. Willis, J. Vac. Sci. Technol. A **16**, 1006 (1998).
[16] P. Molinàs-Mata and J. Zegenhagen, Phys. Rev. B **47**, 10 319 (1993).
[17] For a discussion of the Mn diffusion barriers, see: W. Zhu, H.H. Weitering, E.G. Wang, E. Kaxiras, and Z.Y. Zhang, Phys. Rev. Lett. **93**, 126102 (2004).
[18] N.D. Lang, Phys. Rev. B **34**, 5947 (1986).
[19] H.H. Woodbury and W.W. Tyler, Phys. Rev. **100**, 659 (1955).
[20] A. Depuydt, C. van Haesendonck, N.S. Maslova, V.I. Panov, S.V. Savinov, and P.I. Arseev, Phys. Rev. B **60**, 2619 (1999).
[21] M.M.R. Evans, J.C. Glueckstein, and J. Nogami, Phys. Rev. B **53**, 4000 (1996).
[22] T. Nagao, S. Ohuchi, Y. Matsuoka, and S. Hasegawa, Surf. Sci. **419**, 134 (1999).
[23] C.S. Fadley, D.A. Shirley, A.J. Freeman, P.S. Bagus, and J.V. Mallow, Phys. Rev. Lett. **23**, 1397 (1969).
[24] C.S. Fadley and D.A. Shirley, Phys. Rev. A **2**, 1109 (1970).
[25] J.H. van Vleck, Phys. Rev. **45**, 405 (1934).
[26] S. Doniach and M. Šunjić, J. Phys. C **3**, 285 (1970).
[27] The ^7S and ^5S intensity ratio is robust against the choice of the background function.
[28] V.R. Galakhov, M. Demeter, S. Bartkowski, M. Neumann, N.A. Ovechkina, E.Z. Kurmaev, N.I. Lobachevskaya, Y.M. Mukovskii, J. Mitchell, and D.L Ederer, Phys. Rev. B **65**, 113102 (2002).